20th AIAA Computational Fluid Dynamics Conference
27 - 30 June 2011, Honolulu, Hawaii

AIAA 2011-3382

Three-Dimensional MHD on Cubed-Sphere Grids: Parallel Solution-Adaptive Simulation Framework

L. Ivan* and H. De Sterck†

Applied Mathematics Department, University of Waterloo

200 University Ave. W., Waterloo, Ontario, N2L 3G1, Canada

S. A. Northrup‡ and C. P. T. Groth§

University of Toronto Institute for Aerospace Studies

4925 Dufferin Street, Toronto, Ontario, M3H 5T6, Canada

An accurate, effcient and scalable cubed-sphere grid framework is described for simulation of magnetohydrodynamic (MHD) space-physics flows in domains between two concentric spheres. The unique feature of the proposed formulation compared to existing cubed-sphere codes lies in the design of a cubed-sphere framework that is based on a genuine and consistent multi-block implementation, leading to flux calculations, adaptivity, implicit solves, and parallelism that are fully transparent to the boundaries between the six grid root blocks that correspond to the six sectors of the cubed-sphere grid. Crucial elements of the proposed approach that facilitate this flexible design are: an unstructured connectivity of the six root blocks of the grid, multi-dimensional k-exact reconstruction that automatically takes into account information from neighbouring cells, and adaptive division of the six root blocks into smaller blocks of varying resolution that are all treated exactly equally for ghost cell information transfers, flux calculations, adaptivity, implicit solves and parallel distribution. The approach requires significant initial investment in developing a general and sophisticated adaptive multi-block implementation, with the added complexity of unstructured root-block connectivity, but once this infrastructure is in place, a simulation framework that is uniformly accurate and easily scalable can be developed naturally, since blocks that are adjacent to sector boundaries or sector corners are not treated specially in any way. The general design principles of the adaptive multi-block approach are described and, in particular, how they are used in the implementation of the cubed-sphere framework. The finite-volume discretization, parallelization, and implicit solves are also described. The adaptive mesh refinement (AMR) algorithm uses an upwind spatial discretization procedure in conjunction with limited linear solution reconstruction and Riemann-solver based flux functions to solve the governing equations on multi-block hexahedral mesh. A flexible block-based hierarchical data structure is used to facilitate automatic solution-directed mesh adaptation according to physics-based refinement criteria. The parallel implicit approach is based on a matrix-free inexact Newton method that solves the system of discretized nonlinear equations and a preconditioned generalized minimal residual (GMRES) method that is used at each step of the Newton algorithm. An additive Schwarz global preconditioner in conjunction with local block-fill incomplete lower-upper (BFILU) type preconditioners provides robustness and improves convergence efficiency of the iterative method. The Schwarz preconditioning and block-based data structure readily allow efficient and scalable parallel implementations of the implicit AMR approach on distributed-memory multi-processor architectures. Numerical test problems, including grid convergence studies and realistic global modelling of solar wind conditions, are discussed to demonstrate the accuracy and efficiency of the proposed solution procedure.

*Postdoctoral Fellow, Email: livan@math.uwaterloo.ca, Member AIAA.
†Associate Professor, Email: hdesterck@uwaterloo.ca.
‡PhD Candidate, Email: northrup@utias.utoronto.ca.
§Professor, Email: groth@utias.utoronto.ca, Senior Member AIAA.

I. Introduction & Motivation

With ever-increasing human activity in space and the dependency of human society on the well-functioning of technological systems in space and on Earth, high-performance computational methods for space-physics modelling are desirable for the real- or faster than real-time prediction of eruptive space-weather events such as solar flares and coronal mass ejections (CME),[1] and their influence on the terrestrial environment. Numerical solutions of the equations arising in the modelling of these very complex flows are computationally intensive and feasible only on massively parallel computers.[1–3] One of the main numerical challenges is provided by the presence of a wide variety of temporal and length scales on which interesting plasma physics occurs throughout the large domains associated with large-scale space-weather phenomena. Therefore, scalable high-performance algorithms capable of resolving the solution features of these flows with a reduced number of computational elements and of greatly reducing the time required to obtain numerical solutions of these problems are actively researched.

This work considers the development and application of an implicit second-order Godunov-type finite-volume method in a scalable massively-parallel three-dimensional block-based adaptive mesh refinement (AMR) implementation for prediction of compressible space-plasma flows governed by the ideal magnetohydrodynamics (MHD) equations and influenced by gravitational fields. Despite providing only an approximate description of plasma behaviour (i.e., ideal MHD models neglect kinetic effects, ignore resistivity and diffusion, and treat ions and electrons as a single fluid), the equations of ideal MHD are relatively sufficiently accurate to be used for global MHD simulations and have been successfully employed to simulate many important space-plasma processes.[2,3] As such, the computational framework proposed herein represents a starting point for the development of an MHD-based capability that can be successfully applied on massively parallel computational clusters (i.e. on the order of 10,000-30,000 processing cores) to the prediction of complicated space-physics flows of the type encountered in space-weather phenomena.

The simulation of many space-physics flows requires the discretization of spherical shell geometries, and the choice of the grid is important in formulating an efficient and accurate numerical method for solving partial differential equations on such domains. Although they are a natural choice, spherical-polar grids raise numerical difficulties associated with the presence of pole singularities and consequently, may negatively impact the accuracy and performance of the numerical procedure.[4,5] Alternatively, a potentially more efficient implementation can be obtained based on cubed-sphere grids,[6] which recently emerged as a technique aimed to overcome some of the disadvantages with current latitude-longitude grid constructs. In a two-dimensional (2D) cubed-sphere grid, the surface of a sphere is represented free of any strong singularities as the projection of a cube onto the spherical surface which results in six adjoining grid faces (or sectors) that seamlessly cover the whole sphere. Although eight weak singularities are created at the projection of the cube corners, the resulting cubed-sphere grid is still far more uniform than a polar grid in terms of shape and size of the cells. The six grid faces lend themselves naturally to a multi-block mesh data structure and allow the discretization to be carried out with structured grids, thereby permitting easier implementation of competitive numerical schemes. In the same fashion, a three-dimensional (3D) cubed-sphere grid is obtained by overlaying a sequence of concentric 2D spherical shell grids in the radial direction and forming six three-dimensional blocks, each of which is enclosed by the union of four radial and two spherical faces. Note that the quasi-uniform and self-similar multi-block nature of the cubed-sphere grid makes it ideally suited for implementation on massively parallel architectures and for performing block-based adaptive mesh refinement. However, implementation of such algorithms is inherently difficult due to the complex inter-block connectivity embedded in adaptive cubed-sphere grids which can only be handled with adequate three-dimensional unstructured connectivity and storage for the solution blocks. Moreover, it is highly desirable that the numerical scheme employed for obtaining solutions to equations discretized on cubed-sphere grids has a multi-dimensional character that provides both robustness and accuracy in the computation of solution gradients, especially near the sector boundaries and in the presence of mesh resolution changes, yet maintains a simplicity that makes it computationally efficient.

Other discretization approaches of spherical shell geometries are also possible either based on rectangular Cartesian grids with embedded spherical boundaries[2,7] or, more generally, based on completely unstructured mesh connectivity. Examples of the latter approaches are the Cartesian cut-cell methods[8] and the geodesic grids generated with different tessellation elements such as the icosahedron.[9] An obvious advantage of the cubed-sphere approach over these methods is that it not only easily allows the generation of fairly regular tessellations of the sphere but it also avoids the numerical complexities and possible inefficiencies, such as irregular access to data in memory, raised by the unstructured nature of the latter methods. Hence, the

logically Cartesian representation of the data structure within each block constituent of the cubed-sphere mesh allows for performing optimizations based on proximate data residing in cache.

Cubed-sphere grids have been already successfully considered for applications to weather and climate modelling[10] as well as to computational astrophysics.[5] More recently, Ullrich *et al.*[11] have proposed a fourth-order finite-volume formulation and applied it to shallow-water equations on the sphere. In addition, Yang *et al.*[12] have also recently considered the solution of 2D shallow water equations on the cubed sphere, and developed a fully implicit Newton-Krylov finite-volume algorithm for this grid topology and carried out parallel performance studies with up to 2,048 processing cores. In fact, Jacobian-free Newton-Krylov methods have been already widely considered for MHD applications, as shown in the recent survey by Knoll and Keyes,[13] including for space-physics simulations on solution-adaptive Cartesian grids.[3]

The large-scale domain decomposition of 3D cubed-sphere meshes is typically obtained by generating multiple cuts in the radial direction, thereby increasing the number of partitioning blocks that can be farmed to different processors to $6 \times N_c$, where N_c is the number of radial blocks in each sector. For 2D spherical geometries Putman and Lin[4] used discretization with spherical patches. Although local enhancement of flow features has been already widely considered in the context of h-adaptation on latitude-longitude spherical grids (see, e.g.,[14]), formulations of three-dimensional adaptive mesh refinement procedures on cubed-sphere grids are not widespread and represent an ongoing research effort. Adaptive mesh refinement is an effective approach for coping with the computational cost of large-scale numerical simulations, such as those encountered in space-physics flows. Computational grids that automatically adapt to the solution of the governing equations are effective in treating problems with disparate length scales, providing the required spatial resolution while minimizing memory and storage requirements. A recent review of the impact of AMR to space-physics simulations, numerical astrophysics and computational cosmology is given by Norman.[15]

An important aspect in the development of numerical algorithms on cubed-sphere grids is related to the treatment of interfaces between adjacent grid blocks, along which grid lines have slope discontinuities. In particular, the type of information shared between the blocks is important for the accuracy and robustness of the numerical method. Several approaches have been proposed in the literature including the direct information transfer from interior cells of neighbouring blocks to layers of overlapping "ghost" cells, the one-dimensional interpolation known as *cascade interpolation* which makes use of some particular features of the cubed-sphere grid,[6] as well as a one-sided reconstruction followed by high-order Gaussian quadrature to determine the average solution data within each ghost element.[11] It should be obvious that within the framework of Godunov-type finite-volume methods the particular choice of interface treatment is ultimately related to how accurate and robust the reconstruction procedure is to the presence of grid irregularities.

In the current work, the parallel block-based AMR framework recently proposed by Gao and Groth[16] for the prediction of turbulent non-premixed combusting flows is extended to space-plasma flows and adaptivity on 3D cubed-sphere grids. Note that currently existing AMR frameworks for space-physics flows are generally Cartesian or spherical-polar based and do not allow for arbitrary hexahedral meshes. Also, the solution procedure described herein seems to be the first application of a block-based AMR algorithm to adaptivity on 3D cubed-sphere meshes. Additionally, a parallel implicit AMR scheme based on the Newton-Krylov-Schwarz algorithm proposed by Northrup and Groth for reacting flows[17,18] is applied to the discretization of the MHD equations on cubed-sphere grid topologies. In what follows, a detailed summary of the proposed multi-block implementation of the cubed-sphere grid and the finite-volume computational framework for hexahedral elements is provided. The accuracy of the numerical procedure is then demonstrated with analytical solutions and with comparisons to highly-accurate one-dimensional (1D) transonic flow solutions obtained with the Newton Critical Point (NCP) method described in.[19] Additionally, numerical results are provided to illustrate the predictive capabilities of the AMR algorithm for magnetized and non-magnetized space-plasma problems, such as spherically-symmetric transonic winds and supersonic bow-shock flows past a sphere. Finally, a more realistic space-physics problem is considered by developing a global MHD model similar to the one proposed by Groth *et al.*[2] for the time-averaged solar wind at minimum solar activity.

II. Governing Equations

In this paper, numerical solutions of the three-dimensional ideal MHD equations for magnetized, inviscid, fully ionized, quasi-neutral and compressible plasmas are considered, which can be expressed in the weak conservation (divergence) form as

$$\frac{\partial \mathbf{U}}{\partial t} + \vec{\nabla} \cdot \vec{\mathbf{F}} = \mathbf{S} + \mathbf{Q}\,, \tag{1}$$

where $\mathbf{U}$, the conserved variable solution vector of density, ρ, momentum, $\rho\vec{V}$, magnetic field, $\vec{B}$, and total energy, ρe, is written as

$$\mathbf{U} = \left[\begin{array}{cccc} \rho, & \rho\vec{V}, & \vec{B}, & \rho e \end{array} \right]^T , \tag{2}$$

the inviscid solution flux dyad, $\vec{\mathbf{F}}$, has the form

$$\vec{\mathbf{F}} = \left[\begin{array}{c} \rho\vec{V}, \\ \rho\vec{V}\vec{V} + (p + \vec{B}\cdot\vec{B}/2)\vec{\vec{I}} - \vec{B}\vec{B}, \\ \vec{V}\vec{B} - \vec{B}\vec{V}, \\ (\rho e + p + \vec{B}\cdot\vec{B}/2)\vec{V} - (\vec{V}\cdot\vec{B})\vec{B} \end{array} \right] , \tag{3}$$

and $\mathbf{S}$, the so-called Powell source term, is given by

$$\mathbf{S} = -\left[\begin{array}{c} 0 \\ \vec{B} \\ \vec{V} \\ \vec{V}\cdot\vec{B} \end{array} \right] \nabla\cdot\vec{B} = \mathcal{S}\,\nabla\cdot\vec{B}\,, \tag{4}$$

the role of which is not only to make the MHD equations Galilean invariant and symmetrizable, as proved by Godunov,[20] but also to provide a numerically stable way of controlling the errors in the divergence free condition, $\nabla\cdot\vec{B} = 0$, a technique first advocated by Powell and co-workers.[21] The column vector $\mathbf{Q}$ contains different volumetric sources arising from the physical modelling of the studied problem as explained below. Note that Eqs.(1)-(4) represent the non-dimensional scaled form of the MHD equations following from the non-dimensionalization described by, e.g., Powell *et al.*[21] and by Groth *et al.*[2] for the solar wind. In Eqs.(2) and (3) the specific total plasma energy is $e = p/(\rho(\gamma-1)) + V^2/2 + B^2/(2\rho)$, where p is the pressure, V is the speed of the flow and B is the magnitude of the magnetic field. The speed of the flow is calculated as $V = \sqrt{v_x^2 + v_y^2 + v_z^2}$ based on the three Cartesian velocity components v_x, v_y and v_z in the x-, y-, and z-coordinate directions. Similarly, the total magnetic field $B = \sqrt{B_x^2 + B_y^2 + B_z^2}$ follows from the Cartesian components B_x, B_y and B_z of the magnetic vector field. The ideal gas equation of state $p = \rho RT$ is assumed, where T is the gas temperature and $R = 1/\gamma$ is the gas constant. For a polytropic gas (thermally and calorically perfect), the ratio of plasma specific heats, γ, is a constant and the specific heats are given by $C_v = 1/(\gamma-1)$ and $C_p = \gamma/(\gamma-1)$. Unless otherwise specified, di-atomic gases are used throughout this paper which corresponds to $\gamma = 7/5 = 1.4$.

Herein, the volumetric source term $\mathbf{Q} = \mathbf{Q}_G + \mathbf{Q}_R + \mathbf{Q}_H + \mathbf{Q}_O$ accounts for sources associated with external gravitational fields, $\mathbf{Q}_G$, rotational effects, $\mathbf{Q}_R$, effects of coronal heating processes and heat and radiation transfer, $\mathbf{Q}_H$, as well as others, $\mathbf{Q}_O$. Note that $\mathbf{Q}_R$ and $\mathbf{Q}_H$ are used only for solar wind modelling whereas $\mathbf{Q}_O$ is used for obtaining a MHD manufactured solution, as described in Sect. V.B.1. A spherically symmetric external gravitational field $\vec{g} = -g_*/r^2\hat{\mathbf{e}}_r$ is considered, where g_* is the non-dimensional gravitational force, r is the normalized distance to the solar or planet center, and $\hat{\mathbf{e}}_r$ indicates the radial unit vector. The non-dimensional gravitational force $g_* = G\,M_*/(l_o\,a_o^2)$ is computed based on the gravitational constant, G, the solar or planetary mass, M_*, the reference length scale, l_o, and the ion-acoustic wave speed, a_o, of a suitable reference solution state. Thus, the volumetric source term $\mathbf{Q}_G$, which accounts for the effect of gravitational acceleration, is expressed as a function of the radial position vector, $\vec{r} = r\hat{\mathbf{e}}_r$, in the following vector form

$$\mathbf{Q}_G = -\frac{\rho g_*}{r^3}\left[0\,, \vec{r}\,, \vec{0}\,, \vec{r}\cdot\vec{V}\right]^{\mathrm{T}} . \tag{5}$$

For solar wind flow calculations, the MHD equations are solved in a frame rotating around the z-coordinate direction with an angular velocity $\vec{\Omega} = \Omega_o(l_o/a_o)\hat{\mathbf{e}}_z$, where Ω_o is fixed and represents an average angular velocity of the Sun (see[2] for details). Thus, the column vector $\mathbf{Q}_R$ for this problem includes the effects of centripetal and Coriolis acceleration forces and takes the following form

$$\mathbf{Q}_R = -\rho\left[0\,, \left[\vec{\Omega}\times\left(\vec{\Omega}\times\vec{r}\right)\right] - 2\vec{\Omega}\times\vec{V}\,, \vec{0}\,, \vec{V}\cdot\left[\vec{\Omega}\times\left(\vec{\Omega}\times\vec{r}\right)\right]\right]^{\mathrm{T}} . \tag{6}$$

To reproduce a realistic solar wind using the ideal MHD description, which neglects the thermal conduction that is so important in the vicinity of the Sun,[22] and to allow the use of an ideal plasma gas with a polytropic index $\gamma = 5/3$ throughout the computational domain such that adiabatic cooling at larger heliospherical distances is correctly modelled, Groth *et al.*[2] have added an extra source term to the energy equation that mimics the effects of heat conduction and energy dissipation above the transition region such that to reproduce solar wind features determined by *in situ* observations. This solar wind model with additional heating source term has proved its use in several numerical simulations of CME evolution[2,23,24] and it is used herein as well, in the same form. Thus, the heating source term $\mathbf{Q}_H$ is given by

$$\mathbf{Q}_H = -\rho \left[0 \, , \vec{0} \, , \vec{0} \, , \rho q \left(T_o - \gamma \frac{p}{\rho} \right) \right]^{\mathrm{T}} \, , \tag{7}$$

where $q(x, y, z)$ is an exponentially-decaying specific heat capacity function of the radial distance from the Sun and $T_o = T_o(x, y, z)$ is a prespecified "target" temperature which has a particular spatial distribution.[23]

The aforementioned equations can be simplified by considering the magnetic field, $\vec{B}$, equal to zero, in which case the flow of the non-magnetized plasma reduces to the Euler equations in non-dimensional form. This simplification has been used in this work for part of the accuracy assessment of the 3D cubed-sphere computational framework using analytical and highly-accurate one-dimensional numerical solutions.

III. Cubed-sphere Grids

Over the last decade various grid generation techniques have been applied to cubed-sphere grids in a quest to obtain the right balance between the degree of orthogonality and uniformity of the grid so as to improve the overall accuracy of the numerical scheme. Starting from the original non-orthogonal cubed-sphere grids[6] based on gnomonic projections, one can produce quasi-orthogonal meshes in exchange of some grid uniformity by using gridding techniques such as elliptic solver generators. Using a particular finite-volume implementation, Putman and Lin[4] evaluate the relative accuracy of four different cubed-sphere grids and conclude that despite its non-orthogonality the gnomonic grid achieves comparable accuracy to that of the conformal and quasi-orthogonal elliptic and spring grids due to its improved uniformity. The key element herein is the ability of the numerical scheme to handle non-orthogonal discretizations.

The generation of the cubed-sphere meshes used in this work is also based on gnomonic projection due to its implementation simplicity and minimum impact on the application of a block-based mesh refinement algorithm to these tessellations. In particular, the angularly equidistant mapping described in[6] is used to generate the initial six blocks of our mesh. In this equiangular projection, the equiangular coordinates, ξ and η, are defined individually for each of the six cubed-sphere sectors and chosen to span the range $[-\pi/4, \pi/4]$ to describe completely the spherical geometry of a particular sector for a given radius, r. An example of a cubed-sphere grid with six blocks of $16 \times 16 \times 30$ cells generated in this way is shown in Fig. 1. Although this example depicts a uniform mesh in the radial direction, stretching techniques can be employed in our implementation to improve the radial mesh resolution in different domain areas. Note also that the multi-dimensional character of our finite-volume numerical procedure (see Sect. IV.A) allows for a non-differential treatment of the highly non-orthogonal regions near the spherical projections of the eight cube corners.

Although the level of 3D connectivity required by the cubed-sphere grid has not been explored in previous AMR applications with our framework,[16,17] the flexible block-based hierarchical tree-like data structure of the AMR implementation allows for natural accommodation of the complex topology of the multi-block cubed-sphere grids. As such, a list of pointers provides access to the data of each logically Cartesian (i.e. structured) solution block while the flexible octree data structure keeps track of the refinement level and connectivity between the solution blocks in an unstructured way. In particular, an unstructured root-block connectivity is used to define the relative relationships among the six initial cubed-sphere blocks which lie at the top-level of the octree and form the so-called root blocks. To uniquely define the orientation of the geometric elements of the hexahedral blocks as well as the inter-block connectivity, an abstract notation based on cardinal directions is used. Correspondingly, Fig. 1(b) illustrates the face connectivity for each of the four faces (denoted as West (W), South (S), East (E) and North (N)) of all six blocks that make up the basic cubed-sphere grid. Although the root blocks (i.e. the initial six) do not have any neighbours at the top and bottom, as those faces represent the physical boundaries of the domain and correspond to the outer and inner spheres, this is not true in general for a block created in the process of mesh adaptation.

For computational domains that do not completely cover the sphere it is still possible to obtain a dis-

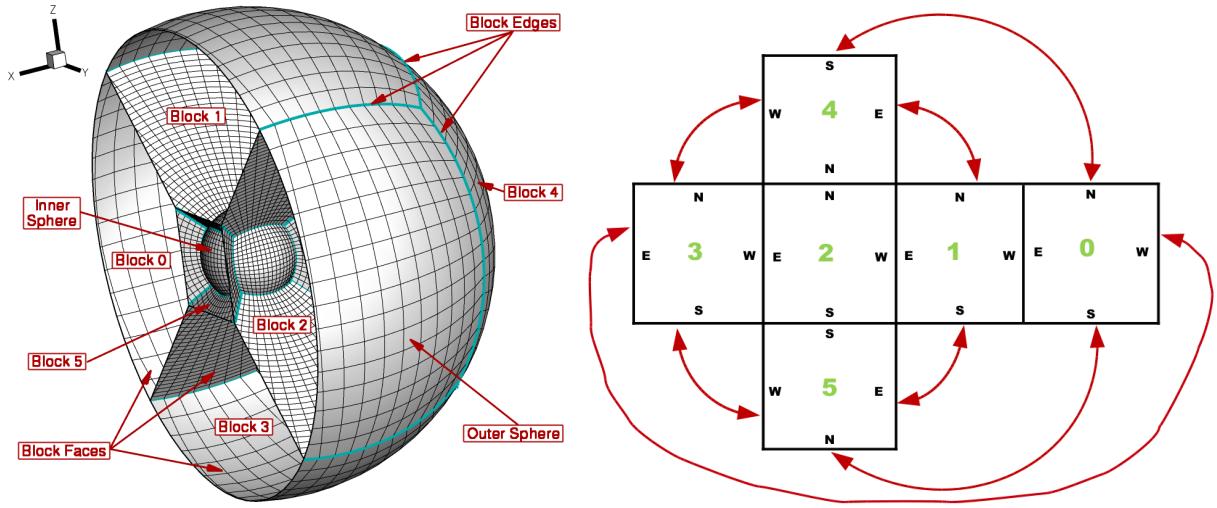

(a) Cross-section of the cubed-sphere grid

(b) Illustration of connectivity among blocks

Figure 1. Three-dimensional cubed-sphere grid with six blocks and depiction of inter-block connectivity.

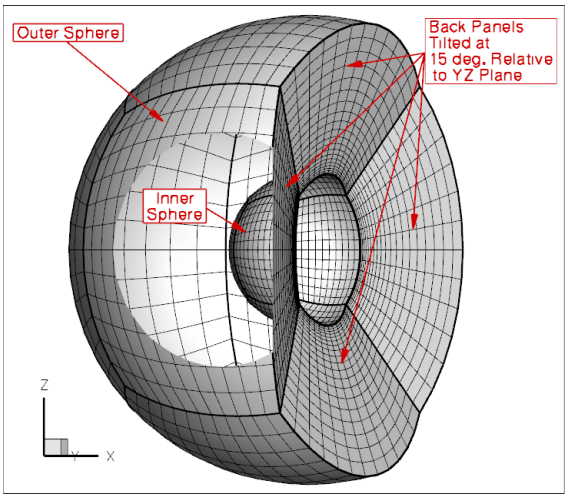

Figure 2. Cubed-sphere grid formed by only five root blocks, for simulation on one side of the sphere. A cut in the outer spherical geometry allows a better view of the inner spherical cap.

cretization based on the cubed-sphere approach by eliminating the unnecessary blocks and modifying accordingly the range of values for the equiangular coordinates, ξ and η, of the included blocks. An example of such a domain discretization is shown in Fig. 2, in which case one root block is removed and the planar domain boundaries are tilted at 15° relative to the Cartesian (y,z) plane. Note that this mesh thus contains only five blocks instead of the typical six associated with a complete cubed-sphere mesh. This extra flexibility in our implementation allowed us to better resolve interesting flow features occurring in front of the sphere with a smaller domain and fewer computational cells as compared to the case in which the domain at the back of the sphere would have been included.

IV. Parallel Implicit AMR Scheme

IV.A. Finite-Volume Discretization

Numerical solutions of Eq. 1 are sought here by applying a Godunov-type finite-volume spatial discretization procedure[25] in conjunction with second-order polynomial reconstruction and Riemann-solver based flux functions. Thus, the set of coupled ordinary differential equations (ODEs) resulting from the application of

a finite-volume formulation to Eq. 1 for cell (i, j, k) of a multi-block mesh composed of hexahedral computational cells is given by

$$\frac{d\mathbf{U}_{i,j,k}}{dt} = -\frac{1}{V_{i,j,k}} \sum_{m=1}^{N_f} \left(\vec{\mathbf{F}} \cdot \vec{n}\, \Delta A\right)_{i,j,k,m} + \bar{\mathbf{S}}_{i,j,k} + \bar{\mathbf{Q}}_{i,j,k} = \mathbf{R}_{i,j,k}(\mathbf{U})\,, \tag{8}$$

where $V_{i,j,k}$ is the cell volume, N_f is the total number of faces, and $\vec{n}$ and ΔA are the unit outward normal vector and the area of cell-face m, respectively. The numerical fluxes, $\vec{\mathbf{F}} \cdot \vec{\mathbf{n}}$, at the mid point of each face of cell (i, j, k) are determined from the solution of a Riemann problem. Given the left and right interface solution states, $\mathbf{U}_l$ and $\mathbf{U}_r$, an upwind numerical flux is evaluated by solving a Riemann problem in the direction defined by the normal to the face. The initial solution states, $\mathbf{U}_l$ and $\mathbf{U}_r$, are determined by performing the multi-dimensional limited piecewise linear solution reconstruction proposed by Barth[26] in conjunction with either Barth-Jespersen[26] or Venkatakrishnan[27] slope limiters. The least-squares solution of the linear reconstruction is based on a symmetric three-dimensional supporting stencil which generally includes 27 cells in total. For a corner cell near the point where three blocks meet the reconstruction stencil is formed with only 24 cells. Note that this multi-dimensional reconstruction procedure seems to perform both accurately and robustly on cubed-sphere grids, thereby allowing the use of direct information transfer between neighbouring blocks for inter-block communication and avoiding any special treatment of the cells near block sector boundaries. In our computational studies the Lax-Friedrichs[28] and HLLE,[29] including the modified HLLE version due to Linde,[30] approximate Riemann solvers have been used. The numerical procedure outlined above results in a second-order upwind finite-volume scheme. The average value of the Powell source term, $\bar{\mathbf{S}}_{i,j,k}$, of cell (i, j, k) is computed with second-order accuracy by estimating the quantity $\mathcal{S}$ based on the appropriate cell-averaged solution variables (i.e., the value of the reconstructed polynomial at the cell centroid) and multiplying it with the following discretization for $\nabla \cdot \vec{B}$:

$$\left(\nabla \cdot \vec{B}\right)_{i,j,k} = \frac{1}{V_{i,j,k}} \sum_{m=1}^{N_f} \left(\vec{B}_f \cdot \vec{n}\, \Delta A\right)_{i,j,k,m}\,, \tag{9}$$

where $\vec{B}_f$ is an interface magnetic field computed as the arithmetic mean of the left and right reconstructed values, that is $\vec{B}_f = \left(\vec{B}_l + \vec{B}_r\right)/2$. The contribution of all other volumetric sources to the solution residual, $\mathbf{R}_{i,j,k}$, is also evaluated with second-order accuracy by computing the average source term $\bar{\mathbf{Q}}_{i,j,k}$ at the centroid of cell (i, j, k) .

To obtain the steady-state solutions of the problems considered in this work, the coupled system of nonlinear ODEs given by Eq. 8 has been solved using the parallel implicit Newton-Krylov-Schwarz algorithm described in Sect. IV.C in combination with multi-stage explicit time-marching schemes[31] for the start-up.

IV.B. Parallel Block-Based AMR

As previously mentioned, a flexible block-based hierarchical data structure is used in conjunction with the spatial discretization procedure described above to facilitate automatic solution-directed mesh adaptation on body-fitted multi-block cubed-sphere mesh. The general AMR framework allows for anisotropic mesh refinement and an efficient and highly scalable parallel implementation has been achieved via domain partitioning.[17] Mesh adaptation is accomplished by refining and coarsening appropriate solution blocks. In regions requiring increased cell resolution, a "parent" block is refined by dividing itself into eight "children" or "offspring". Each of the eight octants or sectors of a parent block becomes a new block having the same number of cells as the parent and thereby doubling the cell resolution in the region of interest. The additional mesh nodes in the new fine blocks are inserted in-between the nodes inherited from the parent. This process can be reversed in regions that are deemed over-resolved and eight children are coarsened into a single parent block. The mesh refinement is constrained such that the grid resolution changes by only a factor of two between adjacent blocks. An important fact with regard to cubed-sphere grids is that the unstructured root block connectivity allows naturally to have three blocks meeting in a corner, which is the case at the eight weak singularities. Local refinement and coarsening of the mesh is directed according to the so-called physics-based refinement criteria. In particular, for the test cases considered here, density gradient and divergence and curl of velocity are used in the decision to refine or coarsen a solution block.

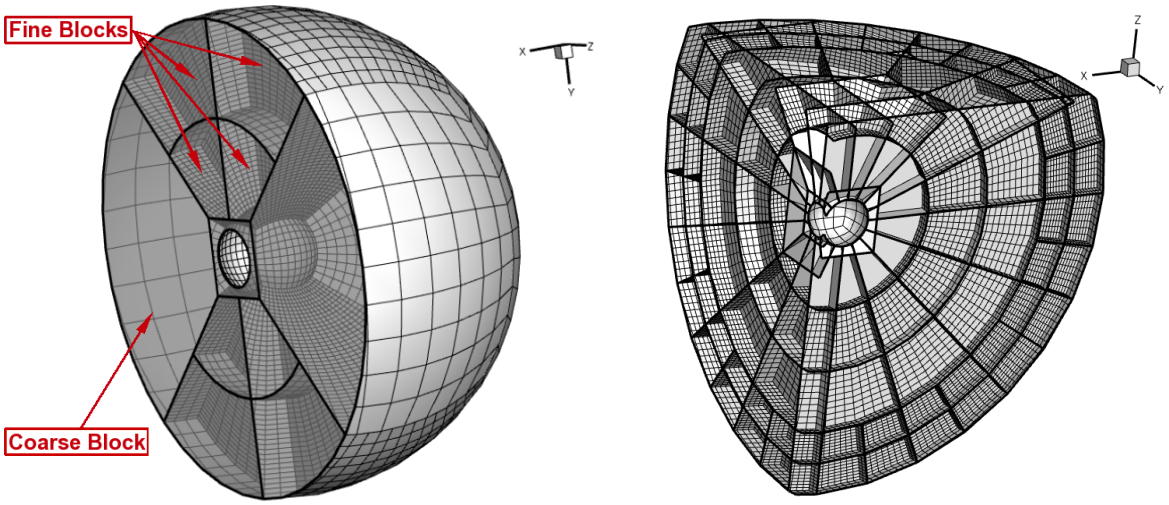

(a) Cross-section of a cubed-sphere grid with one refinement level

(b) Complex cut into an adapted cubed-sphere grid with a few refinement levels

Figure 3. Illustration of three-dimensional block-based adapted cubed-sphere grids showing the block boundaries and the associated meshes.

The solution procedure is used in conjunction with standard multi-grid-type restriction and prolongation operators to evaluate the solution on all blocks created by the coarsening and division processes, respectively.

In order that the finite-volume scheme can be applied to all blocks in a more independent manner, some solution information is shared between adjacent blocks having common interfaces. This information is stored in additional layers of overlapping "ghost" cells associated with each block. Two layers of ghost cells are sufficient for second-order accuracy. At interfaces between blocks of equal resolution, these ghost cells are simply assigned the solution values associated with the appropriate interior cells of the adjacent blocks. At resolution changes, restriction and prolongation operators, similar to those used in block coarsening and division, are employed to evaluate the ghost cell solution values. Within the AMR approach, additional inter-block communication is also required at interfaces with resolution changes to strictly enforce the flux conservation properties of the finite-volume scheme.[32,33] In particular, the interface fluxes computed on more refined blocks are used to correct the interface fluxes computed on coarser neighbouring blocks and ensure the solution fluxes are conserved across block interfaces. A detailed description of our block-based AMR algorithm for multi-block hexahedral mesh is provided in the recent work by Groth and co-workers.[16,17]

Two illustrative examples for the application of the AMR algorithm described above to cubed-sphere grids are shown in Fig. 3. Note that the AMR procedure in the cubed sphere case can be used both to enhance local solution features but also to improve the parallelization of the algorithm via domain decomposition with more than six blocks. Note also that a body-fitted mesh approach is obtained in this case by simply ensuring that newly inserted mesh nodes at the inner and outer spherical boundaries belong to the appropriate spherical shell.

An efficient domain partitioning is achieved in our implementation by distributing equally the solution blocks making up the computational mesh among available processors, with more than one block permitted per processor. The combination of this scalable domain decomposition and the effective AMR-based block-multiplication procedure allowed us to perform efficient parallel calculations for this research with more than 2,000 processor cores.

IV.C. Newton-Krylov-Schwarz (NKS) Method

A parallel implicit approach is used to find steady-state solutions to the discrete form of the MHD equations governing space-plasma flows. In our approach, which is based on the formulation of Northrup and Groth[17,18] for laminar reacting flows, Newton's method is used to solve the coupled set of nonlinear ODEs given by Eq. 8. A preconditioned generalized minimal residual (GMRES) method is then used to solve the resulting system of linear equations at each step of the Newton algorithm. An additive Schwarz preconditioner is used in combination with local block incomplete lower-upper (BILU) preconditioning to improve performance of

the linear iterative solver. A short description of the approach outlined above is provided next.

Applying Newton's method to the residual equation, $\mathbf{R}(\mathbf{U}) = 0$, the following linear system of equations

$$\left(\frac{\partial \mathbf{R}}{\partial \mathbf{U}}\right)^n \triangle \mathbf{U}^n = \mathbf{J}^n \Delta \mathbf{U}^n = -\mathbf{R}(\mathbf{U}^n), \tag{10}$$

is obtained for the solution change $\Delta \mathbf{U}^n = \mathbf{U}^{n+1} - \mathbf{U}^n$ at Newton iteration level n. Using an initial estimate, $\mathbf{U}^n = \mathbf{U}^0$, successively improved estimates for the solution, $\mathbf{U}^{n+1}$, are obtained by solving Eq. 10 at each step, n, of the Newton method, where $\mathbf{J}$ is the modified residual Jacobian. The iterative procedure is repeated until an appropriate norm of the solution residual is sufficiently small, i.e., $||\mathbf{R}(\mathbf{U}^{n+1})||_2 < \epsilon ||\mathbf{R}(\mathbf{U}^0)||_2$ where ϵ is some small parameter (typically, $\epsilon \approx 10^{-12}$–$10^{-10}$). Each step of Newton's method requires the solution of a system of linear equations of the form $\mathbf{Jx} = \mathbf{b}$. This system is large, sparse, and non-symmetric and a preconditioned GMRES method[34,35] is used for its solution. Preconditioning is required for the linear solver to be effective. Right preconditioning of the form $(\mathbf{JM}^{-1})(\mathbf{Mx}) = \mathbf{b}$ is used here where $\mathbf{M}$ is the preconditioning matrix. An additive Schwarz global preconditioner with variable overlap[13,35,36] is used in conjunction with local BILU preconditioners for each sub-domain. The local preconditioner is based on a block ILU(f) or BILU(f) factorization of an approximate Jacobian for each subdomain. Here, f is the level of fill. Note that the approximate residual Jacobian incorporates analytical knowledge only about the flux Jacobian, $\frac{\partial \vec{\mathbf{F}}}{\partial \mathbf{U}}$, and the gravitational source Jacobian, $\frac{\partial \mathbf{Q}_G}{\partial \mathbf{U}}$, and as such the current preconditioner may be less effective in the presence of other sources. As the GMRES algorithm does not explicitly require the evaluation of the global Jacobian matrix, $\mathbf{J}$, a so-called "matrix-free" or "Jacobian-free" approach can be adopted and is used here. Thus, numerical differentiation based on Fréchet derivatives is used to approximate the matrix-vector product $\mathbf{JM}^{-1}\mathbf{x}$.

V. Numerical Results

A set of numerical results demonstrating the accuracy and capability of the aforementioned approach is now described for a range of flow problems obtained with the magnetized and non-magnetized plasma. Results for both fixed and AMR meshes are included.

V.A. Results for Non-Magnetized Plasma

V.A.1. Spherically Symmetric Transonic Wind

To illustrate the accuracy of the algorithm for solar wind-like solutions, the expansion of an inviscid compressible non-magnetized plasma gas under the influence of a gravitational field is now considered. Similar test cases have been studied in[19] and the method outlined there for one-dimensional problems has been used here to provide a highly accurate reference solution for our 3D simulation. As in,[19] normalization factors have been used to provide non-dimensional variables. The spherically symmetric subsonic inflow at the inner sphere $R_i = 1$ is defined by the dimensionless density $\rho = 5$ and pressure $p = 23$. The gravitational invariant has been chosen $GM_* = 14$ which allows for a stationary transonic outflow solution in which the radial flow velocity is initially subsonic, then passes through a critical point where the local Mach number is one, and subsequently takes on supersonic values beyond the critical radius. Although a crude approximation of a real solar wind, the accurate capturing of the transonic behaviour outlined above is still representative of this space-physics problem and it represents an important milestone towards performing more realistic simulations.

The predicted Mach number distribution for this spherically symmetric transonic flow obtained on a uniform cubed-sphere mesh M3 with 1,228,800 cells is shown in Fig. 4(a). In this case, 128 cells are used to resolve the radial direction. Inflow and outflow boundary conditions have been specified for this test case and the solution of a Riemann problem at the boundaries ensures the correct propagation of the flow characteristics, thereby allowing the solution residual to converge to machine accuracy. The result shows that the steady-state transonic solution has been correctly captured and the Mach number contour lines are close to circular indicating a good homogeneity of the flow solution at this grid resolution.

In Fig. 4(b) the flow properties of the predicted solution sampled along the X-axis are compared against those obtained with the NCP method on a non-uniform grid so as to capture the sharp density and pressure gradients near the inflow boundary. Additionally, the radial velocity prediction in the same direction obtained

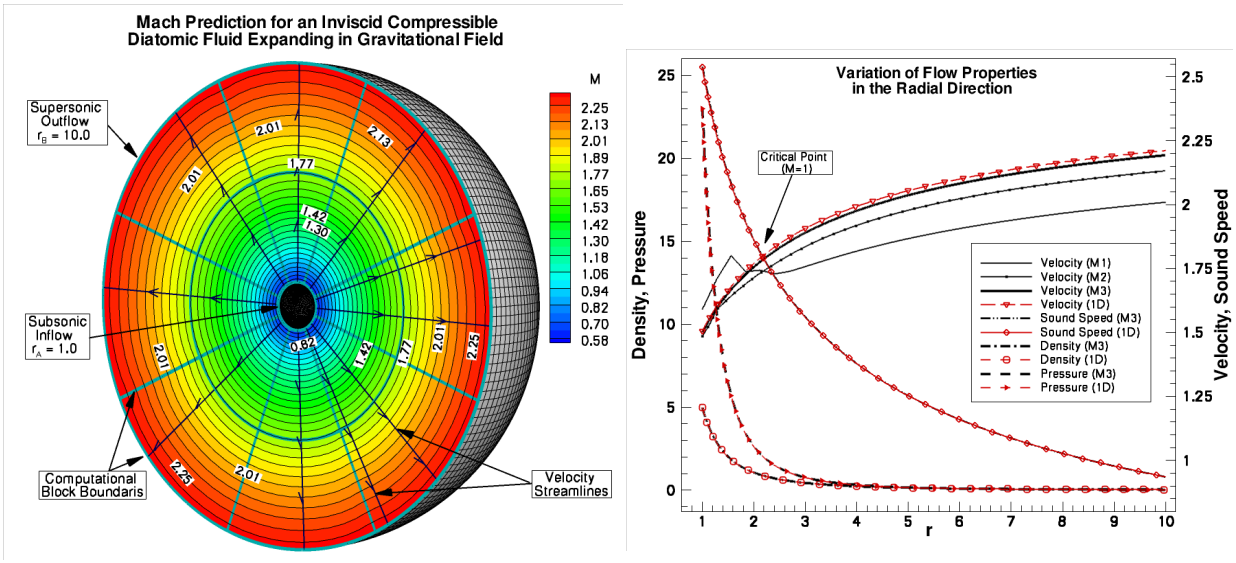

(a) (b)

Figure 4. (a) Predicted Mach number distribution for spherically symmetric transonic wind obtained on the uniform mesh M3 with 1,228,800 cells; and (b) variation of flow properties in the X-axis direction predicted on M3 are compared against those obtained with the NCP method in one-dimension. The velocity prediction on meshes M1 and M2 (see text) is also shown.

with the mesh M1 and M2 with 19,200 and 153,600 cells, respectively, has been also plotted. Note that these two meshes have 32 and 64 cells, respectively, in the radial direction. It is quite noticeable that, the solution significantly improves as the mesh is refined and approaches in the convergence limit the 1D transonic solution predicted by the NCP method. Note also that the density and pressure variables are better predicted everywhere as compared to the radial velocity, most likely due to the fact that their values have been imposed at the inflow boundary.

To assess the capability of the computational framework to improve the prediction of flow properties in regions of large solution gradients and the accuracy of the critical point location, the same transonic wind problem has been reconsidered with automatic solution-directed mesh adaptation. The initial mesh in this case consisted of 48 blocks, each of which with $6\times6\times16$ cells. The contour plot of the Mach number obtained on the refined mesh after five levels of refinement applied to the 3D cubed-sphere grid is shown in Fig. 5(a). The block boundaries shown in the same figure indicate that a fairly symmetric refinement is automatically generated so as to improve the prediction of solution gradients near the inflow boundary, and demonstrate that the proposed AMR approach can be successfully applied to three-dimensional cubed-sphere grids. However, a slight deviation from spherical symmetry also occurs most likely due to the fact that the solution gradients used by the refinement criteria are better resolved in those regions with smaller mesh spacing, a direct consequence of the slight grid non-uniformity in a cubed-sphere mesh. Other refinement criteria which may avoid this are currently under investigation. The comparison of flow properties predicted by the 1D NCP method and the 3D AMR algorithm described in this work along the X-axis are shown in Fig. 5(b). It is quite obvious that the two solutions show excellent agreement in the transonic region and only slight deviations are encountered close to the supersonic outflow due to reduced resolution in the adaptive grid. Note however that the under-resolved supersonic outflow in this case is only a consequence of the parameters used for the gradient-based refinement criteria and does not represent a limitation of the AMR framework.

V.A.2. Supersonic Flow Past Sphere

The application of the proposed AMR algorithm to the solution of supersonic flow past a sphere is now considered to illustrate the predictive capabilities on 3D adaptive cubed-sphere grids. The free-stream Mach number is $M_\infty = 2.0$ and the inner and outer spheres have been positioned at $R_i = 1$ and $R_o = 32$, respectively. The predicted density distributions on the final mesh consisting of 10,835 blocks and 8,321,280 computational cells is shown in Fig. 6. Each grid block consists of $8\times8\times12$ cells and the AMR efficiency after 7 levels of

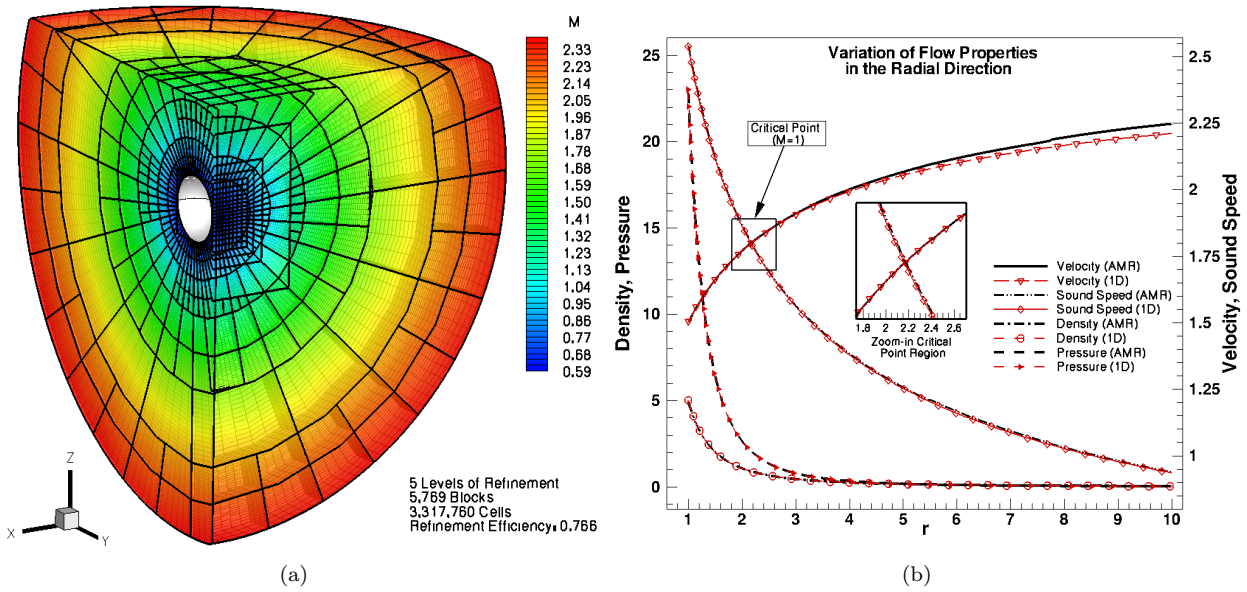

(a) (b)

Figure 5. (a) Predicted Mach number distribution for spherically symmetric transonic wind obtained on the adapted cubed-sphere mesh after 5 refinement levels and with 3,317,760 cells; and (b) the flow properties in the X-axis direction are compared against those predicted with the NCP method.

refinement is 0.993. The result clearly shows that the three-dimensional bow shock and shocks arising at the base of the sphere are correctly identified by the gradient-based refinement criteria and well resolved by the AMR procedure. However, the bow shock in front of the sphere is better resolved than on the sides, where the gradients are smaller, pointing to the necessity to consider better refinement criteria in the future. Nevertheless, the application of the algorithm to this purely three-dimensional problem demonstrates the validity of the proposed body-fitted block-based AMR approach to adaptation on cubed-sphere grids.

V.B. Results for Magnetized Plasma

V.B.1. Systematic Grid Convergence Studies Based on MHD Manufactured Solution

To assess the accuracy of the upwind finite-volume scheme on cubed-sphere grids, uniform convergence studies with a time-invariant axisymmetric manufactured solution for a magnetized gas at supersonic inflow conditions have been performed. In this problem, the volumetric source term $\mathbf{Q}$ in Eq.(1) includes only the

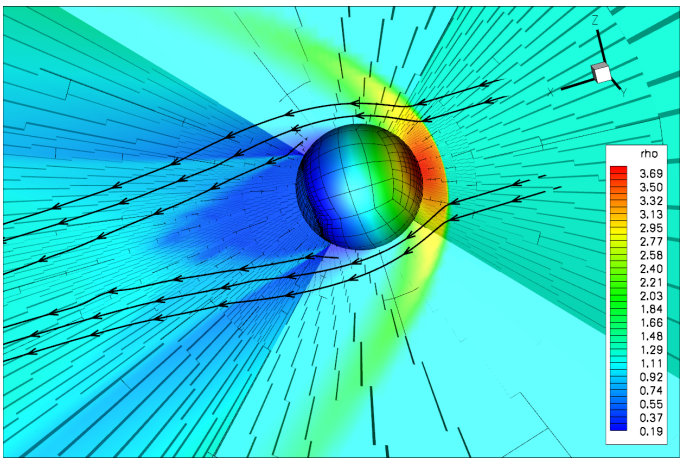

Figure 6. Predicted density distribution for $M = 2.0$ flow past a sphere obtained on the final refined AMR mesh with 10,835 blocks. The block boundaries of the multi-block AMR grid are shown with solid line on the interior spherical surface and with shaded lines in the rest of the domain. A few streamlines are also shown.

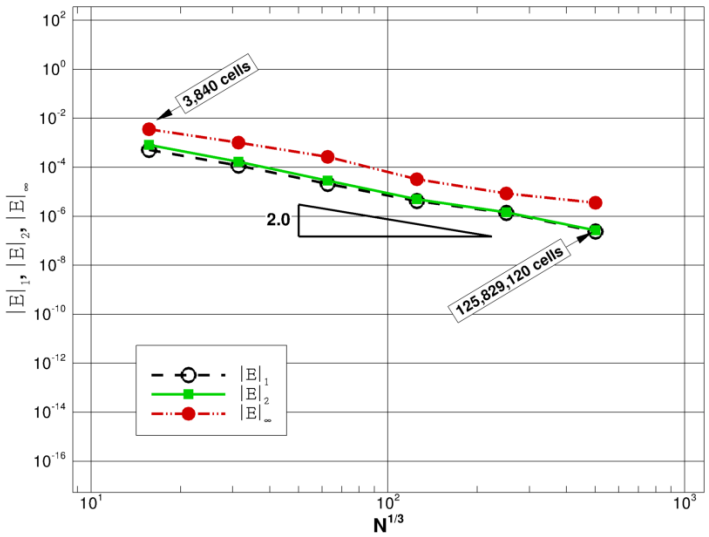

Figure 7. L_1, L_2, **and** L_∞ **error norms in the predicted solution density for the manufactured MHD solution described in the text.**

term $\mathbf{Q}_O$, which represents the analytical residual obtained for the following exact solution:

$$\mathbf{U}(x,y,z) = \left[\; r^{-\frac{5}{2}}, \;\; \frac{x}{\sqrt{r}}, \;\; \frac{y}{\sqrt{r}}, \;\; \frac{z}{\sqrt{r}} + \kappa r^{\frac{5}{2}}, \;\; \frac{x}{r^3}, \;\; \frac{y}{r^3}, \;\; \frac{z}{r^3} + \kappa, \;\; r^{-\frac{5}{2}} \; \right]^T, \tag{11}$$

where $\kappa = 0.017$ is a perturbation parameter chosen such that the solution has significant latitudinal variation yet the flow remains free of any discontinuities. As can be easily observed from Eq.(11), the velocity and the magnetic fields have been chosen aligned everywhere such that $\vec{V}\times\vec{B} = 0$ and therefore, no source terms arise in the induction equation. Moreover, the magnetic field has been constructed by considering a background inverse squared radial function, $\vec{B}_0 = r^{-2}\hat{\mathbf{e}}_r$, plus a perturbation field, $\vec{B}_1 = \nabla f$, derived from the first-order spherical harmonic function $f(x,y,z) = \kappa z$, and thus to automatically satisfy the divergence free condition. This magnetic field is also irrotational and consequently, the magnetic pressure and magnetic tension in the momentum equation are zero.

Thus, the final form of $\mathbf{Q}_O$ for a di-atomic gas is a function only of the space coordinates and can be written as

$$\mathbf{Q}_O = \begin{bmatrix} 0, \\ \frac{1}{2}xr^{-\frac{5}{2}}\left(r^{-1} - 5r^{-2} - \kappa z\right), \\ \frac{1}{2}yr^{-\frac{5}{2}}\left(r^{-1} - 5r^{-2} - \kappa z\right), \\ \frac{1}{2}zr^{-\frac{5}{2}}\left(r^{-1} - 5r^{-2} - \kappa z\right) + \frac{5}{2}r^{-\frac{1}{2}}\kappa(1+\kappa r z) + \kappa r^{-\frac{1}{2}}, \\ \vec{0}, \\ \frac{1}{2}r^{-2} + \kappa z(3.5r^{-1} + 2\kappa z) + \frac{(\kappa r)^2}{2}\left(7 + 5\kappa r z\right) \end{bmatrix}. \tag{12}$$

The computational domain used for this convergence study is defined by the inner and outer spheres of radius $R_i = 2$ and $R_o = 3.5$, respectively, chosen such that the flow remains superfast everywhere. Consequently, the inflow boundary condition is specified based on the exact solution and the outflow is imposed based on linear extrapolation. These particular choices greatly reduce the time required to obtain the converged numerical solution with machine accuracy.

The L_1, L_2, and L_∞ norms of the error in the predicted solution density at cell centroids obtained on a series of grids ranging in size from 8×8×10 to 256×256×320 cells for each of the six cubed-sphere blocks, which corresponds to 3,840 and 125,829,120 total cells, respectively, are given in Fig. 7 for this supersonic flow. The results show that the second-order theoretical accuracy for this smooth flow is achieved in all error norms as the mesh is refined, indicating that the finite-volume algorithm handles accurately the non-orthogonal grid near the projection of the cube corners and at sector boundaries. As the mesh is refined, the slopes of the L_1-, L_2- and L_∞-norms approach in the asymptotic limit -2.06, -2.10 and -2.05, respectively.

This test problem has also been used to determine the potential savings generated by the use of the NKS implicit algorithm over an explicit solve. A comparison between the computational time and the equivalent

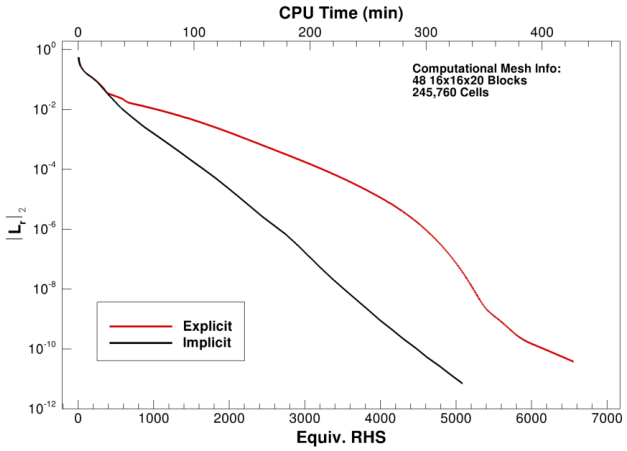

Figure 8. Comparison of explicit and NKS implicit algorithms for the number of equivalent residual evaluations and the computational time, obtained on Intel Xeon E5540 architecture, required to achieve a specific L_2-norm of the solution residual.

number of solution residual (i.e., $\mathbf{R}(\mathbf{U})$) evaluations associated with each of the two algorithms versus the L_2-norm of the solution residual is depicted in Fig. 8 for a cubed-sphere computational mesh with 48 16×16×20 blocks and 245,760 cells. The results show that for relatively low norms of the solution residual (i.e., on the order of $10^{-6}-10^{-8}$) the implicit NKS algorithm improves the computational efficiency of the calculation by about a third of the CPU time required by an explicit solve. Improved computational efficiency can be expected from the NKS algorithm for this problem when used in conjunction with a more effective GMRES preconditioner that accounts for all the source terms present, however this was not the focus of the current work and will be considered in the future. Nevertheless, the current study highlights some of the potential computational savings offered by the use of the implicit formulation in our 3D cubed-sphere framework.

V.B.2. Magnetically Dominated MHD Bow Shock

The application of the proposed AMR algorithm to the solution of uniform supersonic flow past a sphere is considered again. In this case, 3D MHD bow-shock flows around a perfectly conducting sphere and corresponding to magnetically dominated upstream conditions are investigated in conjunction with solution-adaptive cubed-sphere grids. The inflow parameters used for this problem have been selected from[37] and are $\rho=1,\ p=0.2,\ B_x=1,\ B_y=0,\ v_x=1.4943$ and $v_y=0.1307$, which correspond to an upstream plasma characterized by $\beta=2p/B^2=0.4$, an Alfvénic Mach number $M_{Ax}=1.49$ along the upstream magnetic field lines and an angle $\theta_{vB}=5^\circ$ between the upstream velocity and magnetic vector fields. As shown in,[37] this particular upstream configuration gives rise to 3D intermediate shocks and multiple interacting shock fronts, that are sought here to be well resolved by an adaptive mesh refinement procedure.

The computational domain for solving this problem is similar to the one depicted in Fig. 2 and defined by the inner and outer spheres of radius $R_i=1$ and $R_o=8$. Reflection boundary conditions (BCs) are imposed along the inner sphere while a free-stream boundary condition is applied to the outer one. Linear extrapolation BCs are implemented for the back panels of the outer boundary based on the fact that the flow is superfast at those locations and all eight characteristic waves leave the domain. The initial multi-block grid for this problem consists of a total of 20 8×8×10 blocks which are equally divided among four spherical radial cuts, each of which contains five blocks.

The predicted Mach number and density distribution in the Cartesian (x,y) plane obtained after 7 refinement levels on the final refined mesh consisting of 22,693 blocks and 14,523,520 computational cells is shown in Fig. 9. The results show that all shocks arising in front of the sphere are captured by the refinement criteria and are well resolved by the 3D adaptation procedure on cubed-sphere grids, especially in the region corresponding to the bifurcation of the shocks.

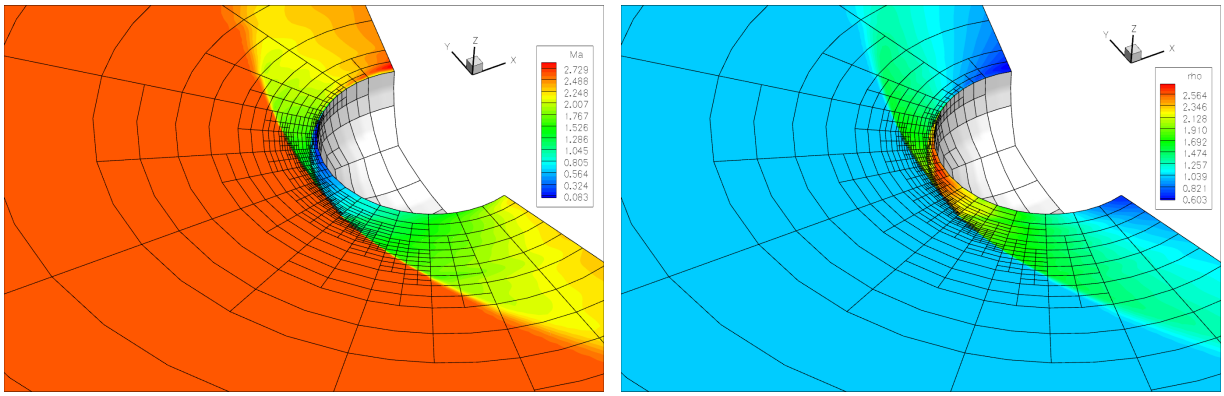

(a) (b)

Figure 9. Predicted (a) acoustic Mach number and (b) density distribution in the Cartesian (x,y) plane for a magnetically dominated supersonic flow past a sphere obtained on the adapted cubed-sphere mesh after 7 refinement levels and with 22,693 blocks and 14,523,520 computational cells, respectively. Additionally, the block boundaries are depicted with solid black lines.

V.B.3. Time-Invariant Solar Wind Solution

Finally, the application of the algorithm to a more realistic space-physics problem is considered. Global MHD models for solar wind modelling and CME propagation have been already developed and investigated in different configurations.[1,2,23,38,39] Thus, the global MHD simulation attempted herein does not aim to improve the predictions already reported for this very challenging space-physics problem, but rather to represent a more comprehensive test for the cubed-sphere simulation framework proposed herein. As such, it represents an initial step towards developing more sophisticated models for the solar wind and carrying out more advanced and complete studies with our algorithm.

A numerical solution of the "steady" solar wind representative of solar minimum conditions (i.e., for the quiet Sun) has been obtained in this research based on the global 3D MHD model of Groth *et al.*[2] Different from the ideal MHD formulation employed in[2] the equations solved in the current implementation do not include a separation of the magnetic field into intrinsic and deviatoric components, an approach first employed by Tanaka[40] to alleviate the necessity of resolving the often large spatial magnetic field gradients present in space physics. The steady-state solar wind from 1 R_s (i.e., solar radius) to nearly 1/2 AU is modelled here by assuming that, at 1 R_s, the inner solar corona is a large, rigidly rotating reservoir of hot plasma with an embedded magnetic multipole field described by a multipole expansion that includes terms up to the octupole moment (see[2,23] for details). The plasma temperature (the sum of the ion and electron temperatures) of the reservoir is assumed to be $T_s = 2.0 \times 10^6$ K, and the plasma density is taken to be 1.5×10^{14} m^{-3}. The solar magnetic field is azimuthally symmetric about the magnetic axis which is aligned with the rotational direction, and both axes coincide with the Cartesian z-coordinate direction. The multipole expansion has been chosen such as to obtain a maximum field strength of 8.4 G at the magnetic poles and a strength of 2.2 G at the solar magnetic equator. The single-fluid plasma has the average particle mass taken to be $\mu = 0.6\, m_p$ to account for the small quantity of helium present in the mixture,[22] where m_p is the proton mass, and a polytropic index $\gamma = 5/3$ is used everywhere in the domain.

For this numerical simulation the computational domain was the spherical shell defined in the rotating frame by the inner and outer spheres of radius $R_i = 1$ and $R_o = 100$, which represent distances normalized by the solar radius, R_s. The cubed-sphere computational grid was stretched with a higher density of grid cells towards the inner sphere and consisted of 48 self-similar $24 \times 24 \times 26$ blocks and 718,848 cells, providing an average angular resolution of 3.75° and a minimum cell size at the solar surface of 1/10 R_s. Boundary conditions are implemented at the inner sphere, where the flow is subslow, according to the propagation of the characteristics, to conservation principles for radial mass and magnetic fluxes, and to physical conditions for the directions of velocity and magnetic field vectors in perfectly conducting fluids (see, e.g.,[39] for details). Moreover, linear extrapolation of density and pressure gradients at inner boundary has been used and plasma was permitted to freely leave the reservoir, but no "backflow" was allowed. At the outer boundary, the flow is superfast and consequently all variables are simply extrapolated. The initial condition for the simulation

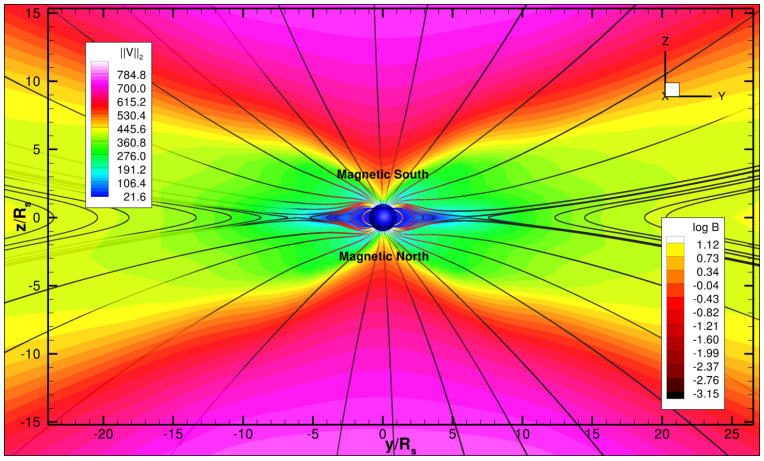

Figure 10. Representation of the steady-state solar wind solution in the (y,z) meridional plane. The colour shading represents the magnitude of the velocity vector, $||\vec{V}||_2$, in km/s and the solid lines are magnetic field lines coloured based on the magnitude of $\log(B)$. The magnetic polarity chosen for this problem is also indicated in the figure.

was provided by Parker's isothermal solar wind[41] and the magnetic field variation has been obtained with the aforementioned multipole expansion.[2]

Figure 10 shows a meridional cut through the numerical solution of the steady-state solar wind obtained using the algorithm described above. The shading represents the magnitude of the velocity field, $||\vec{V}||_2$, and the solid lines correspond to the predicted field lines which have been coloured based on the logarithm of the magnitude of the magnetic field, $\log(B)$. Inspection of Fig. 10 reveals a bimodal outflow pattern with slow wind leaving the Sun near the equator, and high-speed solar wind of around 800 km/s in the regions of open magnetic field lines emanating from the coronal holes. This is an important feature of the solar wind which has been confirmed by *in situ* observations.[2] Other noticeable features present in the solution are the formation of a "helmet streamer" configuration with associated neutral point and equatorial current sheet. It can also be observed that in the regions of close field lines near the solar surface the predicted plasma velocity is very small and subsonic, in the range of 50-100 km/s.

VI. Discussion and Concluding Remarks

A parallel block-based adaptive simulation framework has been proposed for three-dimensional cubed-sphere grids and space-physics flows. The method represents an extension of the recently proposed AMR approach for combusting flows by Gao and Groth.[16] The gnomonic cubed-sphere grid in conjunction with body-fitted block-based AMR has been shown to provide a suitable framework for multi-dimensional finite-volume discretization on three-dimensional spherical shells. The approach calls for better refinement criteria which are less sensitive to the non-uniformity of the cubed-sphere grid and reliably capture three-dimensional flow features. The accuracy of the algorithm has been assessed based on a MHD manufactured exact solution and shown to achieve the theoretical second-order convergence. Moreover, the ability of the scheme to adequately handle and resolve strong discontinuities/shocks has been demonstrated. Furthermore, the predictive capabilities of the proposed framework have been illustrated for simple but relevant transonic solutions obtained for non-magnetized space plasmas. The algorithm has been shown to provide accurate predictions for such problems as compared to highly accurate one-dimensional results. Finally, a global 3D MHD model has been applied on cubed-sphere mesh to obtain steady-state solar wind predictions to distances up to 1/2 AU. The last case study represents a first attempt towards performing more complex and detailed investigations of space-physics problems with the proposed framework, including CME propagation from the solar surface out to distances beyond 1 AU, on three-dimensional time-dependent adaptive cubed-sphere grids. Furthermore, future research will involve application of the algorithm to other complex space-physics problems, the evaluation of the parallel performance of the algorithm on thousands of computing cores, the formulation of more effective GMRES preconditioners for the NKS algorithm and the extension of the numerical scheme to high-order accuracy (i.e., accuracy higher than second-order).

Acknowledgements

This work was supported by CSA (Canadian Space Agency) CGSM Contract No. 9F007-080157/001/ST. Computations were performed on the GPC supercomputer at the SciNet HPC Consortium. SciNet is funded by: the Canada Foundation for Innovation under the auspices of Compute Canada; the Government of Ontario; Ontario Research Fund - Research Excellence; and the University of Toronto.

References

[1]Manchester IV, W. B., Vourlidas, A., Tóth, G., Lugaz, N., Roussev, I. I., Sokolov, I. V., Gombosi, T. I., Zeeuw, D. L. D., and Opher, M., "Three-dimensional MHD Simulation of the 2003 October 28 coronal mass ejection: comparison with LASCO coronagraph observations," *Astrophys. J.*, Vol. 684, 2008, pp. 1448–1460.

[2]Groth, C. P. T., De Zeeuw, D. L., Gombosi, T. I., and Powell, K. G., "Global Three-Dimensional MHD Simulation of a Space Weather Event: CME Formation, Interplanetary Propagation, and Interaction with the Magnetosphere," *J. Geophys. Res.*, Vol. 105, No. A11, 2000, pp. 25,053–25,078.

[3]Gombosi, T. I., Powell, K. G., Zeeuw, D. L. D., Clauer, C. R., Hansen, K. C., Manchester, W. B., Ridley, A. J., Roussev, I. I., Sokolov, I. V., Stout, Q. F., and Tóth, G., "Solution-Adaptive Magnetohydrodynamics for Space Plasmas: Sun-to-Earth Simulations," *Comp. Sci. & Eng.*, Vol. 6, No. 2, 2004, pp. 14–35.

[4]Putman, W. M. and Lin, S.-J., "Finite-volume transport on various cubed-sphere grids," *J. Comput. Phys.*, Vol. 227, 2007, pp. 55–78.

[5]Fragile, P. C., Lindner, C. C., Anninos, P., and Salmonson, J. D., "Application of the cubed-sphere grid to tilted black hole accretion disks," *Astrophys. J.*, Vol. 691, 2009, pp. 482–494.

[6]Ronchi, C., Iacono, R., and Paolucci, P. S., "The "Cubed Sphere": A New Method for the Solution of Partial Differential Equations in Spherical Geometry," *J. Comput. Phys.*, Vol. 124, 1996, pp. 93–114.

[7]Tóth, G., van der Holst, B., Sokolov, I. V., Zeeuw, D. L. D., Gombosi, T. I., Fang, F., Manchester, W. B., Meng, X., Najib, D., Powell, K. G., Stout, Q. F., Glocer, A., Ma, Y.-J., and Opher, M., "Adaptive numerical algorithms in space weather modeling," *J. Comput. Phys.*, Vol. In Press, Corrected Proof, 2011, pp. –.

[8]Aftomis, M. J., Berger, M. J., and Melton, J. E., "Robust and Efficient Cartesian Mesh Generation for Component-Base Geometry," *AIAA J.*, Vol. 36, No. 6, 1998, pp. 952–960.

[9]Giraldo, F. X., "High-order triangle-based discontinuous Galerkin methods for hyperbolic equations on a rotating sphere," *J. Comput. Phys.*, Vol. 214, 2006, pp. 447–465.

[10]Levy, M. N., Nair, R. D., and Tufo, H. M., "High-order Galerkin methods for scalable global atmospheric models," *Comput. & Geos.*, Vol. 33, 2007, pp. 1022–1035.

[11]Ullrich, P. A., Jablonowski, C., and van Leer, B., "High-order finite-volume methods for the shallow-water equations on the sphere," *J. Comput. Phys.*, Vol. 229, No. 17, 2010, pp. 6104 – 6134.

[12]Yang, C., Cao, J., and Cai, X.-C., "A fully implicit domain decomposition algorithm for shallow water equations on the cubed-sphere," *SIAM J. Sci. Comput.*, Vol. 32, 2010, pp. 418–438.

[13]Knoll, D. A. and Keyes, D. E., "Jacobian-free Newton-Krylov methods: a survey of approaches and applications," *J. Comput. Phys.*, Vol. 193, 2004, pp. 357–397.

[14]Jablonowski, C., Herzog, M., Penner, J. E., Oehmke, R. C., Stout, Q. F., van Leer, B., and Powell, K. G., "Block-Structured Adaptive Grids on the Sphere: Advective Experiments," *Mon. Wea. Rev.*, Vol. 134, 2006, pp. 3691–3713.

[15]Norman, M. L., "The Impact of AMR in Numerical Astrophysics and Cosmology," *Lecture Notes in Computational Science and Engineering*, Vol. 41, Springer Berlin Heidelberg, 2005, pp. 413–430.

[16]Gao, X. and Groth, C. P. T., "A parallel solution-adaptive method for three-dimensional turbulent non-premixed combusting flows," *J. Comput. Phys.*, Vol. 229, 2010, pp. 3250–3275.

[17]Northrup, S. A. and Groth, C. P. T., "Prediction of Unsteady Laminar Flames Using a Parallel Implicit Adaptive Mesh Refinement Algorithm," *Proceedings of the 6th U.S. National Combustion Meeting*, May 2009.

[18]Northrup, S. A. and Groth, C. P. T., "Parallel Implicit AMR Scheme for Unsteady Reactive Flows," *Proceedings of the 18th Annual Conference of the CFD Society of Canada, London, Canada*, May 2010.

[19]De Sterck, H., Rostrup, S., and Tian, F., "A fast and accurate algorithm for computing radial transonic flows," *J. Comput. Appl. Math.*, Vol. 223, No. 2, 2009, pp. 916–928.

[20]Godunov, S. K., "Symmetric Form of the Equations of Magnetohydrodynamics," *Numerical Methods for Mechanics of Continuum Medium,* Siberian Branch of USSR Academy of Sciences, Vol. 1, pp. 26–34.

[21]Powell, K. G., Roe, P. L., Linde, T. J., Gombosi, T. I., and De Zeeuw, D. L., "A Solution-Adaptive Upwind Scheme for Ideal Magnetohydrodynamics," *J. Comput. Phys.*, Vol. 154, 1999, pp. 284–309.

[22]Meyer-Vernet, N., *Basics of the Solar Wind*, Cambridge University Press, 2007.

[23]Manchester IV, W. B., Gombosi, T. I., Roussev, I. I., Ridley, A., Zeeuw, D. L. D., Sokolov, I. V., and Powell, K. G., "Modeling a space weather event from the Sun to the Earth: CME generation and interplanetary propagation," *J. Geophys. Res.*, Vol. 109, No. A0, 2004, pp. 2107–2121.

[24]Lugaz, N., Manchester IV, W. B., and Gombosi, T. I., "The evolution of coronal mass ejection density structures," *Astrophys. J.*, Vol. 627, 2005, pp. 1019–1030.

[25]Godunov, S. K., "Finite-Difference Method for Numerical Computations of Discontinuous Solutions of the Equations of Fluid Dynamics," *Mat. Sb.*, Vol. 47, 1959, pp. 271–306.

[26]Barth, T. J. and Jespersen, D. C., "The Design and Application of Upwind Schemes on Unstructured Meshes," Paper 89-0366, AIAA, January 1989.

[27]Venkatakrishnan, V., "On the Accuracy of Limiters and Convergence to Steady State Solutions," Paper 93-0880, AIAA, January 1993.

[28]Tóth, G. and Odstrčil, D., "Comparison of Some Flux Corrected Transport and Total Variation Diminishing Numerical Schemes for Hydrodynamic and Magnetohydrodynamic Problems," *J. Comput. Phys.*, Vol. 128, 1996, pp. 82–100.

[29]Harten, A., Lax, P. D., and van Leer, B., "On Upstream Differencing and Godunov-Type Schemes for Hyperbolic Conservation Laws," *SIAM Rev.*, Vol. 25, No. 1, 1983, pp. 35–61.

[30]Linde, T., "A practical, general-purpose, two-state HLL Riemann solver for hyperbolic conservation laws," *Int. J. Numer. Meth. Fluids*, Vol. 40, 2002, pp. 391–402.

[31]van Leer, B., Tai, C. H., and Powell, K. G., "Design of Optimally-Smoothing Multi-Stage Schemes for the Euler Equations," Paper 89-1933-CP, AIAA, June 1989.

[32]Berger, M. J. and Oliger, J., "Adaptive Mesh Refinement for Hyperbolic Partial Differential Equations," *J. Comput. Phys.*, Vol. 53, 1984, pp. 484–512.

[33]Berger, M. J. and Colella, P., "Local Adaptive Mesh Refinement for Shock Hydrodynamics," *J. Comput. Phys.*, Vol. 82, 1989, pp. 67–84.

[34]Saad, Y. and Schultz, M. H., "GMRES: A Generalized Minimal Residual Algorithm for Solving Nonsymmetric Linear Equations," *SIAM J. Sci. Stat. Comput.*, Vol. 7, No. 3, 1986, pp. 856–869.

[35]Saad, Y., *Iterative Methods for Sparse Linear Systems*, PWS Publishing Company, Boston, 1996.

[36]Gropp, W. D., Kaushik, D. K., Keyes, D. E., and Smith, B. F., "High-Performance Parallel Implicit CFD," *Parallel Computing*, Vol. 27, 2001, pp. 337–362.

[37]De Sterck, H. and Poedts, S., "Intermediate Shocks in Three-Dimensional Magnetohydrodynamic Bow-Shock Flows with Multiple Interacting Shock Fronts," *Phys. Rev. Lett.*, Vol. 84, No. 24, 2000, pp. 5524–5527.

[38]Jacobs, C., van der Holst, B., and Poedts, S., "Comparison between 2.5D and 3D simulations of coronal mass ejections," *Astronomy and Astrophysics*, Vol. 470, 2007, pp. 359–365.

[39]Jacobs, C., *Magnetohydrodynamic modelling of the solar wind and coronal mass ejections*, Ph.D. thesis, University of Leuven, October 2007.

[40]Tanaka, T., "Generation Mechanisms for Magnetosphere-Ionosphere Current Systems Deduced from a Three-Dimensional MHD Simulation of the Solar Wind-Magnetosphere-Ionosphere Coupling Processes," *J. Geophys. Res.*, Vol. 100, No. A7, 1995, pp. 12,057–12,074.

[41]Parker, E. N., "Dynamics of the Interplanetary Gas and Magnetic Fields," *Astrophys. J.*, Vol. 128, No. 3, 1958, pp. 664–676.